Vol.66: e23220101, 2023
https://doi.org/10.1590/1678-4324-2023220101
ISSN 1678-4324 Online Edition

*Article - Engineering, Technology and Techniques*

# A Transformerless Boost-Modified Cuk Combined Single-Switch DC-DC Converter Topology with Enhanced Voltage Gain

**Murali Duraisamy**[1]
https://orcid.org/0000-0002-6890-1687

[1]Government College of Engineering, Department of Electrical and Electronics Engineering, Salem, Tamil Nadu, India.

Editor-in-Chief: Bill Jorge Costa
Associate Editor: Daniel Navarro Gevers

Received: 13-Feb-2022; Accepted: 24-Jan-2023.

*Correspondence: muraliems@gmail.com; Tel.: 0427-2346157 (D.M.).

**HIGHLIGHTS**

- Single-switch configuration for the proposed hybrid converter is employed.
- Static voltage gain of the proposed hybrid topology is improved.
- Power switch is subjected to low voltage-current stress.
- The power conversion efficiency of the proposed converter is improved.

**Abstract:** Recently, the research is towards the development of high static gain DC-DC converters suitable for renewable energy applications. The high voltage gain can be achieved using isolated and non-isolated configurations of the converter. The magnetically coupled inductor based isolated DC-DC converter structures can have improved voltage gain, but they need large size inductors which may lead to increased cost. Thus, the modified structures of non-isolated conventional boost, CUK, and SEPIC topologies with inclusion of additional controlled and uncontrolled switches along with large number of passive components are employed to achieve the improved voltage gain. However, it leads to increased complexity and control. Hence, the researchers concentrated on development of hybrid non-isolated DC-DC converter topologies capable of achieving enhanced static voltage gain, without adding extra controlled switches and passive elements. In this paper, a hybrid non-isolated single-switch DC-DC converter structure is proposed for achieving high voltage gain than that of traditional non-isolated topologies. The proposed hybrid structure operating in continuous inductor current mode is obtained by connecting the conventional boost and the modified CUK converters in parallel. The power switch and the diodes have low voltage-current stress. The operation of the proposed hybrid topology during various modes is explored. The mathematical modeling of the proposed converter is also provided. The MATLAB / SIMULINK study of the suggested hybrid converter has been implemented. The digital simulation study proves the feasibility of the proposed hybrid converter concept and its steady-state behavior.

**Keywords:** boost converter; continuous inductor current mode; Cuk topology; duty ratio; hybrid DC-DC converter topology; MATLAB/SIMULINK; static voltage gain; voltage-current stress.

## INTRODUCTION

In recent times, the commercial, industrial, and domestic consumers of electricity require increased energy demand globally. Both the conventional and non-conventional energy sources are available to meet out the increased energy demand. The use of highly expensive conventional fossil fuels for electrical energy generation results in pollution of environment globally and rapid increase of global average surface temperature [1,2]. These issues can be tackled by using non-conventional energy sources that are renewable, cost-effective and pollution-free. However, the individual performance of the renewable energy sources (RES) for independent electricity generation is lacking due to their intermittent nature [3]. This issue can be solved using hybrid renewable energy systems (HRES) where two or more renewable energy sources are integrated for high quality power generation [4]. The DC output voltage delivered by RES will be fluctuating due to the intermittent nature of the sources. It is therefore necessary to get the stabilized voltage output from the HRES, by means of DC-DC power electronic converters [5]. The predominant role of the DC-DC converters is to achieve high voltage gain and to improve the efficiency of the renewable energy generation system. The HRES can supply power to DC loads through a DC-DC converter, and AC loads are fed through a DC-DC converter and an inverter [6]. The overall performance of the grid-tied HRES is influenced by the appropriate selection of an efficient and high gain DC-DC converter topology.

The DC-DC conversion topologies are categorized into isolated and non-isolated structures respectively. The input and output sides of the isolated converter structures are galvanically isolated using a high frequency transformer. The advantages of the isolated converter topologies include high step-up gain with appropriate duty ratio, no effect of the input on the output port due to a common ground, stable output over a wide range of inputs, isolation, and high power conversion efficiency [7-10]. But, the isolated topologies suffer from the drawbacks such as high voltage spikes occurring across the power switches due to the effect of leakage inductance of the transformer, saturation of magnetic core, thermal effect, control complexity, multistage power conversion process, and increased size and cost of the converter. Hence, the efficient non-isolated high static voltage gain DC-DC converter configurations are opted for renewable energy applications [11].

The traditional simple structured and pulse width modulated non-isolated boost, SEPIC, CUK, and ZETA converter topologies can achieve very high voltage gain if the power switches are operated at maximum value of duty ratios [12]. The shortcomings of these traditional single switch topologies include low power conversion efficiency and increased stress across the switching components. The single switch non-isolated converter topologies are modified by adding extra diodes and passive elements in order to improve the voltage gain [13-19]. The researchers have also developed non-isolated topologies with extra power switches, diodes and passive components for enhanced static voltage gain [20,21]. The use of more number of switching and passive devices in the non-isolated topologies proposed in [13-21] leads to the complexity of the power circuit and the control strategy. Hence, the researchers concentrated on developing the hybrid non-isolated single switch DC-DC converter topologies with simple control strategy, high voltage gain capability and high power conversion efficiency [22-24].

In this paper, a hybrid non-isolated single switch high step-up DC-DC converter structure suitable for renewable energy applications is proposed. The hybrid topology employs the parallel combination of traditional boost and modified CUK DC-DC converters [17,18]. The proposed hybrid positive output converter with single power switch is operated in continuous inductor current mode. The power switch and the diodes are subjected to low stress. The output voltage ($V_0$) is obtained as the sum of the voltages appearing across the two series-connected capacitors that are connected in shunt with the proposed converter circuit. The voltage gain of the suggested hybrid converter is greater than that of the other non-isolated topologies [17,18,22].

The remaining part of the paper is structured as follows: The various modes of operation, steady state behavior, mathematical modelling, simulation results and discussion for the proposed hybrid converter are well explained sequentially in subsequent Sections. The conclusion section concludes the features of the proposed research work.

## MODES OF OPERATION OF THE PROPOSED CONVERTER

The configurations of conventional boost DC-DC converter and the modified CUK DC-DC converter are shown in Figure 1(a) and 1(b) [17,18]. The proposed non-isolated hybrid single switch DC-DC converter structure shown in Figure 1(c) is developed by merging the converter topologies shown in Figure 1(a) and 1(b) in such a way that the power switch (S) and the inductor ($L_1$) are kept commonly on the input side and the rest of the CUK circuit components are connected across the terminals ‘a’ and ‘b’ of the conventional boost converter. The load voltage ($V_0$) is obtained as the sum of voltages across the capacitors $C_1$ and $C_4$.

The proposed hybrid topology exhibits improved voltage gain than that of the topologies shown in Figure 1(a), Figure 1(b), and in [21]. Also, the low voltage stress occurs on the power switch and the diodes. The proposed hybrid single switch converter structure with all active and passive components as ideal is operated in three modes with continuous inductor current. The theoretical waveforms of the converter are shown in Figure 3.

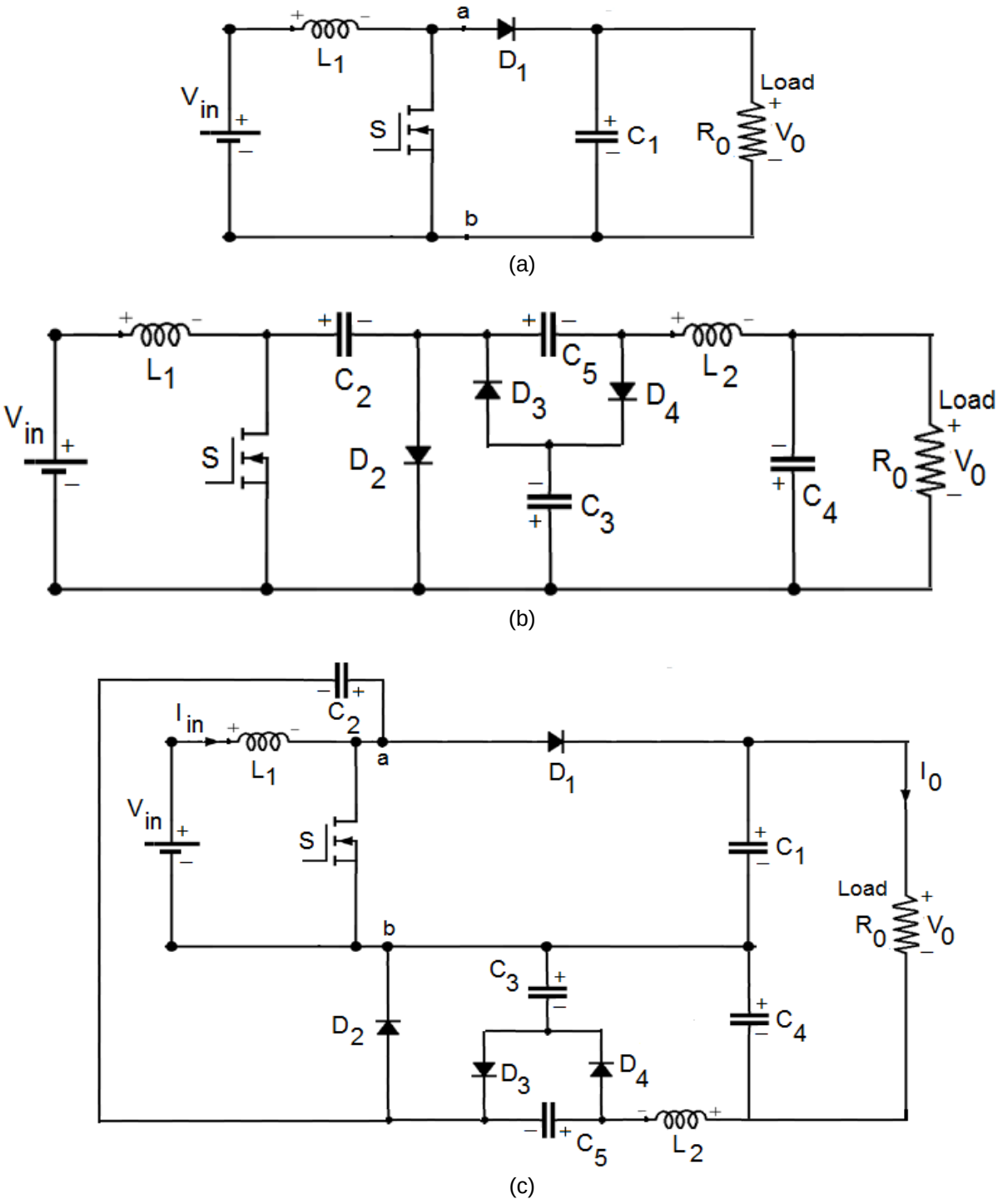


**Figure 1.** Configurations of DC-DC converter. (a). Conventional Boost converter, (b). Modified CUK converter, (c). Proposed hybrid single switch converter

### Mode-I operation ($t_0<t<t_1$):

During the time interval $t_0 – t_1$, the proposed converter operates under Mode-I as shown in Figure 2(a). The power switch S is made to conduct during this interval. The diode $D_3$ gets forward biased and the remaining diodes $D_1$, $D_2$, and $D_4$ get reverse biased. The inductor $L_1$ is charged to the source voltage ($V_{in}$). The capacitor $C_2$ discharges and hence charges the capacitor $C_3$, the capacitor $C_4$, the inductor $L_2$, and the capacitor $C_5$ respectively through two paths: (i). $C_2$-a-S-b-$C_3$-$D_3$-$C_2$, and (ii). $C_2$-a-S-b-$C_4$-$L_2$-$C_5$-$C_2$. The load

$R_0$ receives the current ($I_0$) and hence the voltage ($V_0$) due to the discharge of the capacitor $C_1$. The following Equation (1) is written for the inductors and capacitors.

$$V_{L1} = V_{in}; \qquad V_{L2} = V_{C2} - V_{C4} - V_{C5}; \qquad V_{C2} = V_{C3} \tag{1}$$

where, $V_{L1}$, $V_{L2}$ are the voltages across the inductors $L_1$ and $L_2$; $V_{in}$ is input DC voltage.
$V_{C2}$, $V_{C3}$, $V_{C4}$, & $V_{C5}$ represent respectively the voltages across the capacitors $C_2$, $C_3$, $C_4$, & $C_5$.

**Mode-II operation ($t_1<t<t_2$):**

During the time interval $t_1 - t_2$, the proposed converter operates under Mode-II as shown in Figure 2(b). The power switch S is turned OFF during this interval. The diodes $D_2$ and $D_4$ get forward biased. The diodes $D_1$ and $D_3$ get reverse biased. The inductor $L_1$ discharges and hence charges the capacitor $C_2$ through the path $L_1$-a-$C_2$-$D_2$-$V_{in}$-$L_1$. The passive components $L_2$, $C_3$, $C_4$, and $C_5$ discharge following the two paths: (i). $L_2$-$C_5$-$D_2$-b-$C_4$-$L_2$, and (ii). $L_2$-$D_4$-$C_3$-$C_4$-$L_2$. The load current ($I_0$) is supplied from the capacitor $C_1$. The following Equation (2) is written for the inductors $L_1$ and $L_2$.

$$V_{L1} = V_{in} - V_{C2}; \quad V_{L2} = -V_{C4} - V_{C5} = V_{C3} - V_{C4} \tag{2}$$

**Mode-III operation ($t_2<t<t_3$):**

During the time interval $t_2 - t_3$, the proposed converter operates under Mode-III as shown in Figure 2(c). The power switch S continues to remain in the switched OFF condition. The diode $D_1$ starts to conduct. The diodes $D_2$ and $D_4$ remain conducting. The diode $D_3$ remains reverse biased. The capacitors $C_1$ and $C_2$ are charged by the inductor $L_1$. The load $R_0$ receives power from the source $V_{in}$. The same Equation (2) is written for this Mode-III too in addition to the following equation (3) for the voltage $V_{C1}$ across the capacitor $C_1$.

$$V_{C1} = V_{C2} \tag{3}$$

The Equations (1), (2), & (3) for $V_{C2}$, $V_{L2}$, & $V_{C1}$ give rise to the following Equation (4).

$$V_{C1} = V_{C2} = V_{C3} = -V_{C5} \tag{4}$$

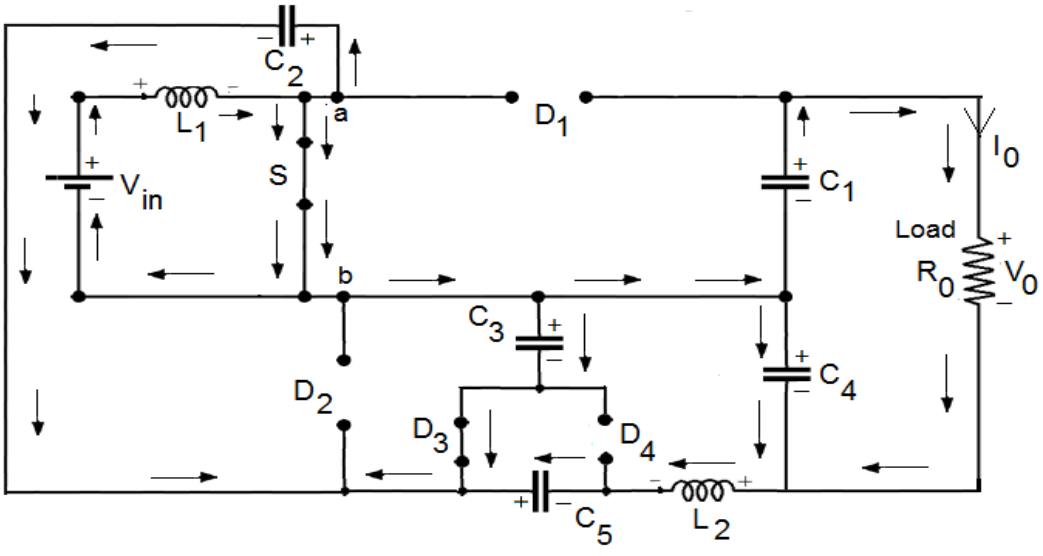


(a)

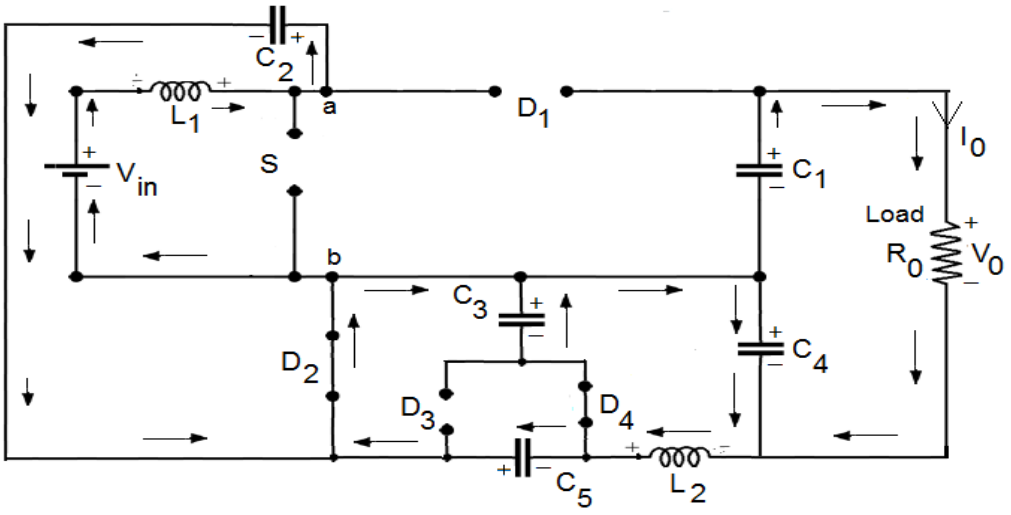


(b)

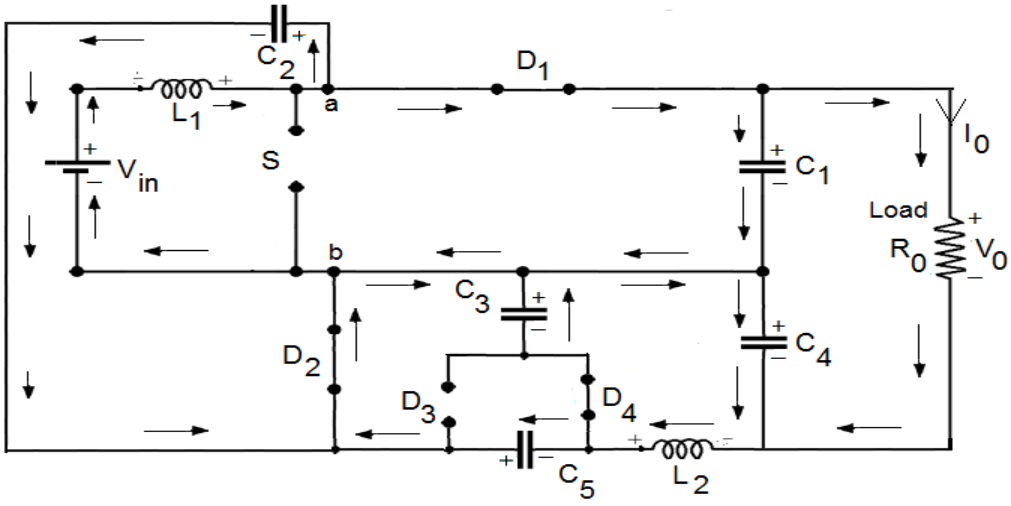


(c)

**Figure 2.** Modes of operation of the proposed DC-DC converter. (a). Mode-I (b). Mode-II (c). Mode-III

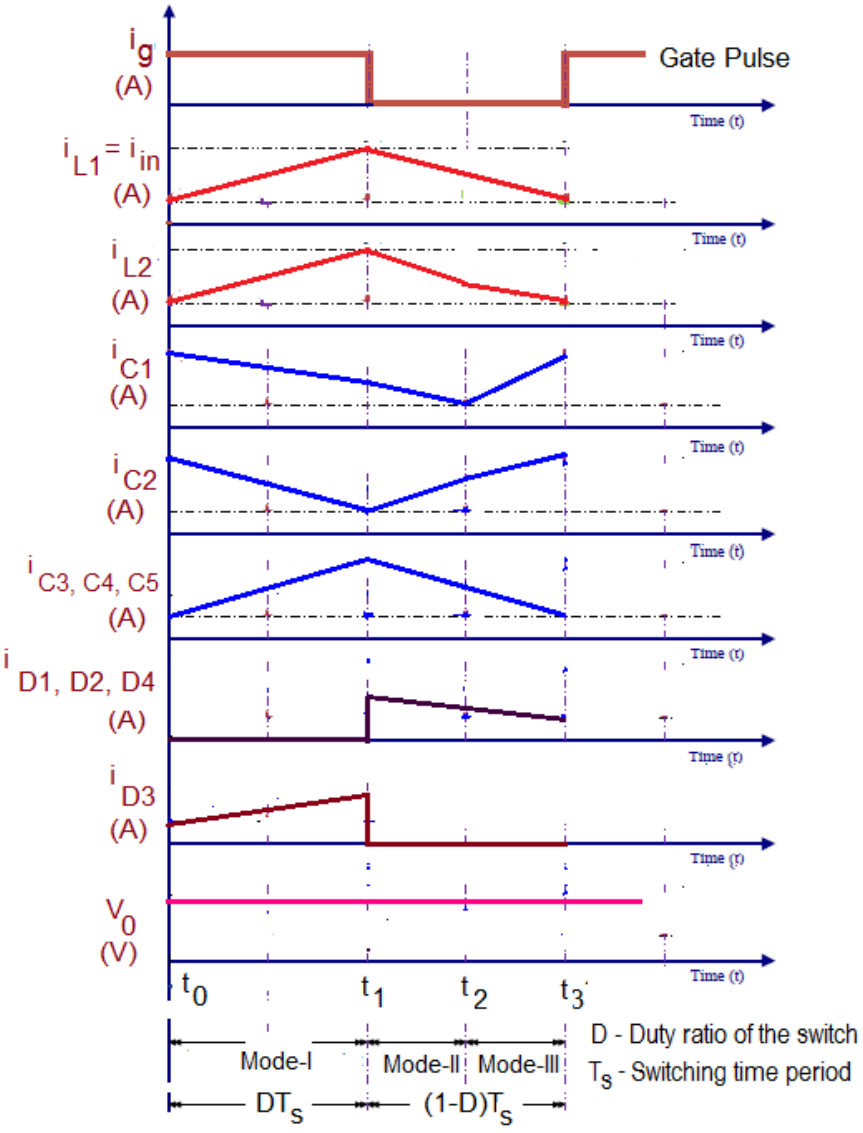


**Figure 3.** Theoretical waveforms of the proposed converter

## STEADY STATE BEHAVIOUR OF THE PROPOSED CONVERTER:

For the conventional boost converter [17] and the modified CUK converter [18] topologies shown in Figure 1(a) and 1(b), with duty ratio 'k' for the power switch, the voltage gain equations are represented as given below:

$$\text{Voltage gain (G) for the conventional boost converter} = \frac{V_0}{V_{in}} = \frac{1}{1-k} \tag{5}$$

$$\text{Magnitude of Voltage gain (G) for the modified CUK converter} = \frac{V_0}{V_{in}} = \frac{1+k}{1-k} \tag{6}$$

For the proposed hybrid DC-DC converter topology, the voltage gain equation is derived using the Equations (1), (2), and (4). The volt-second balance principle is applied to the identical inductors $L_1$ and $L_2$ and the following Equations are obtained.

$$V_{in}kT_s + (V_{in} - V_{C2})(1-k)T_s = 0 \tag{7}$$

$$(V_{C2} - V_{C4} - V_{C5})kT_s + (V_{C3} - V_{C4})(1-k)T_s = 0 \tag{8}$$

From the Equations (4) and (7), the expression for the voltage $V_{C1}$ across the capacitor $C_1$ is obtained.

$$V_{C1} = V_{C2} = V_{C3} = -V_{C5} = \frac{V_{in}}{1-k} \tag{9}$$

From the Equation (8), the expression for the voltage $V_{C4}$ across the capacitor $C_4$ is obtained.

$$V_{C4} = \left(\frac{1+k}{1-k}\right)V_{in} \tag{10}$$

The load voltage ($V_0$) is the sum of the capacitor voltages $V_{C1}$ and $V_{C4}$.

$$V_0 = V_{C1} + V_{C4} = \left(\frac{2+k}{1-k}\right)V_{in} \tag{11}$$

The voltage gain (G) of the proposed hybrid single switch DC-DC converter is obtained as:

$$G = \frac{V_0}{V_{in}} = \frac{2+k}{1-k} \tag{12}$$

The comparison of the voltage gain (G) of the conventional boost converter [17], modified CUK converter [18], hybrid boost and CUK converter [22], and the proposed hybrid single switch DC-DC converter is given in Figure 4. Thus, the proposed hybrid structure provides the improved voltage gain compared to the other topologies. Moreover, the stress on the power switch is found to be low.

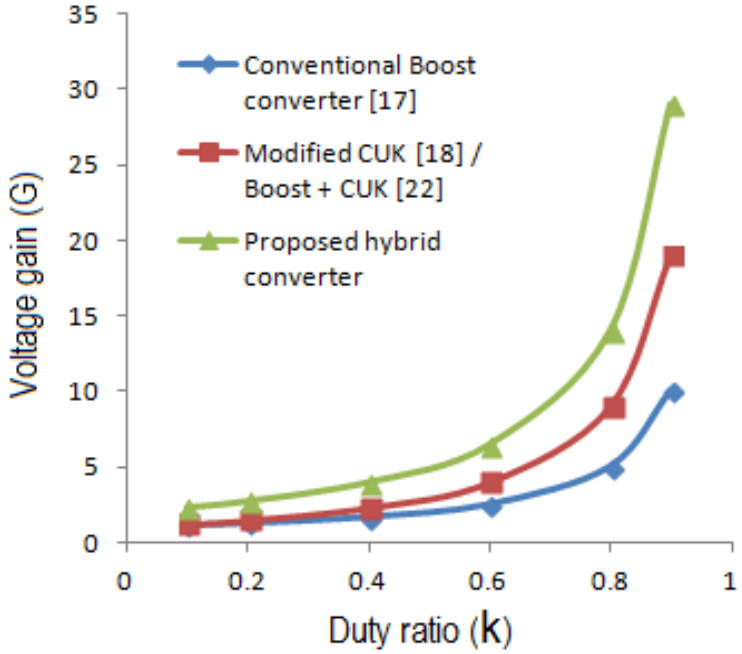


**Figure 4.** Variation of voltage gain (G) of the DC-DC converters with respect to the Duty ratio (k).

By equating the proposed converter input power and output power, the steady state input inductor current $I_{L1}$ is derived as shown below:

$$V_{in}I_{L1} = V_0 I_0; \qquad I_{L1} = \frac{V_0 I_0}{V_{in}} = \left(\frac{2+k}{1-k}\right)I_0 \tag{13}$$

The steady state value of the inductor current $I_{L2}$ is obtained by equating the average value of current through the capacitor $C_4$ to zero during the total switching time period T.

$$I_{C4} = \frac{1}{T}\left(\int_0^{kT}(I_{L2} - I_0)dt + \int_{kT}^{T}(I_{L2} - I_0)dt\right) = 0 \tag{14}$$

From the above equation, $I_{L2}$ is derived as:

$$I_{L2} = I_0 \tag{15}$$

The steady state value of the diode current $I_{D1}$ is obtained by equating the average value of current through the capacitor $C_1$ to zero during the total switching time period T.

$$I_{C1} = \frac{1}{T}\left(\int_0^{kT}(-I_0)dt + \int_{kT}^{T}(I_{D1} - I_0)dt\right) = 0 \tag{16}$$

From the above equation, $I_{D1}$ is obtained as:

$$I_{D1} = \frac{I_0}{(1-k)} \tag{17}$$

The steady state value of the diode current $I_{D2}$ is obtained by equating the average value of current through the capacitor $C_2$ to zero during the total switching time period T.

$$I_{C2} = \frac{1}{T}\left(\int_0^{kT} -(I_{L2} + I_{C3})dt + \int_{kT}^{T}(I_{D2} - I_{L2} + I_{C3})dt\right) = 0 \tag{18}$$

In the above equation, the average value of current through the capacitor $C_3$ is zero during the total switching time period T. Hence, $I_{D2}$ is obtained as:

$$I_{D2} = \frac{I_0}{(1-k)} \tag{19}$$

The steady state value of the diode current $I_{D4}$ is obtained by equating the average value of current through the capacitor $C_5$ to zero during the total switching time period T.

$$I_{C5} = \frac{1}{T}\left(\int_0^{kT} I_{L2}dt + \int_{kT}^{T}(I_{L2} - I_{D4})dt\right) = 0$$

From the above equation, $I_{D4}$ is obtained as:

$$I_{D4} = \frac{I_0}{(1-k)} \tag{20}$$

The steady state value of the diode current $I_{D3}$ is obtained by equating the average value of current through the capacitor $C_2$ to zero during the total switching time period T.

$$I_{C2} = \frac{1}{T}\left(\int_0^{kT} -(I_{L2} + I_{D3})dt + \int_{kT}^{T}(I_{D2} - I_{L2} + I_{D4})dt\right) = 0 \tag{21}$$

From the above equation, $I_{D3}$ is obtained as:

$$I_{D3} = \frac{I_0}{k} \tag{22}$$

The voltage stress across the diodes $D_1$, $D_2$, $D_3$, & $D_4$ are obtained as:

$$\left.\begin{aligned} V_{D1} &= V_{C2} - V_{C1} - V_{C3} = V_{in}\left(\frac{1}{1-k} - \frac{1}{1-k} - \frac{1}{1-k}\right) = -\frac{V_{in}}{(1-k)} \\ V_{D2} &= -V_{C2} = -\frac{V_{in}}{(1-k)}; \quad V_{D3} = -V_{C3} = -\frac{V_{in}}{(1-k)}; \quad V_{D4} = V_{C5} = -\frac{V_{in}}{(1-k)} \end{aligned}\right\} \tag{23}$$

The expressions for the voltage stress ($V_S$) and current stress ($I_S$) of the power switch 'S' are obtained as:

$$V_S = V_{C2} = \frac{V_{in}}{(1-k)} \tag{24}$$

$$I_S = I_{L1} - I_{C2} = I_{L1} - (-(I_{L2} + I_{C3})) \tag{25}$$

In the above expression, $I_{C3} = 0$. Hence, the current stress $I_S$ is obtained as:

$$I_S = \left(\frac{3}{1-k}\right) I_0 \tag{26}$$

The steady state values of voltages and currents for the various circuit components are verified for k = 0.8, $V_{in}$ = 24V, and $I_0 = \frac{P_0}{V_0} = \frac{320}{335}$ = 1 A as shown below using the equations (9), (10), (11), (13), (15), (17), (19), (20), (22), (23), & (25) respectively.

$$V_{C1} = V_{C2} = V_{C3} = -V_{C5} = \frac{V_{in}}{1-k} = \frac{24}{1-0.8} = 120 \text{ V}; \quad V_{C4} = \left(\frac{1+k}{1-k}\right) V_{in} = \frac{24 \times 1.8}{0.2} = 216 \text{ V};$$

$$V_0 = \left(\frac{2+k}{1-k}\right) V_{in} = \frac{2.8 \times 24}{0.2} = 336 \text{ V}; \quad I_{L1} = I_{in} = \left(\frac{2+k}{1-k}\right) I_0 = \frac{2.8 \times 1}{0.2} = 14 \text{ A}; \quad I_{L2} = I_0 = 1 \text{ A};$$

$$I_{D1} = I_{D2} = I_{D4} = \frac{I_0}{(1-k)} = \frac{1}{0.2} = 5 \text{ A}; \quad I_{D3} = \frac{I_o}{k} = \frac{1}{0.8} = 1.25 \text{ A};$$

$$V_S = V_{C2} = \frac{V_{in}}{(1-k)} = 120 \text{ V}; \qquad I_S = \left(\frac{3}{1-k}\right) I_0 = \frac{3 \times 1}{0.2} = 15 \text{ A}.$$

$$V_{D1} = V_{D2} = V_{D3} = V_{D4} = -\frac{V_{in}}{(1-k)} = -\frac{24}{(1-0.8)} = -120\text{V};$$

## MATHEMATICAL MODELLING OF THE PROPOSED HYBRID DC-DC CONVERTER

The state space averaging model of the proposed hybrid single-switch DC-DC converter is derived in this section. During mode-I operation, the switch 'S' is turned ON. The dynamic equations are written as shown below:

$$\left.\begin{aligned} &\frac{di_{L1}}{dt} = \frac{V_{in}}{L_1}; \qquad \frac{di_{L2}}{dt} = \frac{V_{C2}}{L_2} - \frac{V_{C4}}{L_2} - \frac{V_{C5}}{L_2}; \qquad \frac{dV_{C1}}{dt} = -\frac{V_0}{R_0 C_1} = -\frac{(V_{C1} + V_{C4})}{R_0 C_1}; \\ &\frac{dV_{C2}}{dt} = \frac{dV_{C3}}{dt} = -\frac{i_{L2}}{(C_2 - C_3)}; \qquad \frac{dV_{C5}}{dt} = \frac{i_{L2}}{C_5} \\ &y = V_0 = V_{C1} + V_{C4} \end{aligned}\right\} \tag{27}$$

The above equations are written in state space form during ON period of the switch as shown below:

$$\left[\dot{x}\right] = A_1 x + B_1 u; \qquad y = C_1 x + D_1 u \tag{28}$$

Where, $\left[\dot{x}\right] = \left[\dot{i}_{L1} \quad \dot{i}_{L2} \quad \dot{V}_{C1} \quad \dot{V}_{C2} \quad \dot{V}_{C3} \quad \dot{V}_{C4} \quad \dot{V}_{C5}\right]^T$; $\quad [x] = \left[i_{L1} \quad i_{L2} \quad V_{C1} \quad V_{C2} \quad V_{C3} \quad V_{C4} \quad V_{C5}\right]^T$

$$[A_1]=\begin{bmatrix} 0 & 0 & 0 & 0 & 0 & 0 & 0 \\ 0 & 0 & 0 & \frac{1}{L_2} & 0 & -\frac{1}{L_2} & -\frac{1}{L_2} \\ 0 & 0 & -\frac{1}{R_0C_1} & 0 & 0 & -\frac{1}{R_0C_1} & 0 \\ 0 & -\frac{1}{(C_2-C_3)} & 0 & 0 & 0 & 0 & 0 \\ 0 & -\frac{1}{(C_2-C_3)} & 0 & 0 & 0 & 0 & 0 \\ 0 & \frac{1}{C_4} & -\frac{1}{R_0C_4} & 0 & 0 & -\frac{1}{R_0C_4} & 0 \\ 0 & \frac{1}{C_5} & 0 & 0 & 0 & 0 & 0 \end{bmatrix};$$

$$[B_1]=\begin{bmatrix} \frac{1}{L_1} & 0 & 0 & 0 & 0 & 0 & 0 \end{bmatrix}^T;\ [u]=V_{in};\qquad [C_1]=[0\ \ 0\ \ 1\ \ 0\ \ 0\ \ 1\ \ 0];\qquad [D_1]=[0]$$

During mode-II operation of the converter, the switch 'S' is turned OFF. During this period, the following state space model is derived.

$$\left[\dot{x}\right]=A_2x+B_2u;\qquad y=C_2x+D_2u \tag{29}$$

$$[A_2]=\begin{bmatrix} 0 & 0 & 0 & -\frac{1}{L_1} & 0 & 0 & 0 \\ 0 & 0 & 0 & 0 & \frac{1}{L_2} & -\frac{1}{L_2} & 0 \\ 0 & 0 & -\frac{1}{R_0C_1} & 0 & 0 & -\frac{1}{R_0C_1} & 0 \\ \frac{1}{C_2} & 0 & 0 & 0 & 0 & 0 & 0 \\ 0 & \frac{1}{(C_3+C_5)} & 0 & 0 & 0 & 0 & 0 \\ 0 & \frac{1}{C_4} & -\frac{1}{R_0C_4} & 0 & 0 & -\frac{1}{R_0C_4} & 0 \\ 0 & \frac{1}{(C_3+C_5)} & 0 & 0 & 0 & 0 & 0 \end{bmatrix}$$

$$[B_2]=\begin{bmatrix} \frac{1}{L_1} & 0 & 0 & 0 & 0 & 0 & 0 \end{bmatrix}^T;\ [u]=V_{in};\qquad [C_2]=[0\ \ 0\ \ 1\ \ 0\ \ 0\ \ 1\ \ 0];\qquad [D_2]=[0]$$

During mode-III operation of the converter, the switch 'S' remains in the turned OFF condition. During this period the following state space model is derived.

$$\left[\dot{x}\right]=A_3x+B_3u;\qquad y=C_3x+D_3u \tag{30}$$

$$[A_3]=\begin{bmatrix} 0 & 0 & 0 & -\frac{1}{L_1} & 0 & 0 & 0 \\ 0 & 0 & 0 & 0 & \frac{1}{L_2} & -\frac{1}{L_2} & 0 \\ \frac{1}{(C_1+C_2)} & 0 & -\frac{1}{R_0(C_1+C_2)} & 0 & 0 & -\frac{1}{R_0(C_1+C_2)} & 0 \\ \frac{1}{(C_1+C_2)} & 0 & -\frac{1}{R_0(C_1+C_2)} & 0 & 0 & -\frac{1}{R_0(C_1+C_2)} & 0 \\ 0 & \frac{1}{(C_3+C_5)} & 0 & 0 & 0 & 0 & 0 \\ 0 & \frac{1}{C_4} & -\frac{1}{R_0C_4} & 0 & 0 & -\frac{1}{R_0C_4} & 0 \\ 0 & \frac{1}{(C_3+C_5)} & 0 & 0 & 0 & 0 & 0 \end{bmatrix}$$

$$[B_3]=\begin{bmatrix} \frac{1}{L_1} & 0 & 0 & 0 & 0 & 0 & 0 \end{bmatrix}^T; \quad [u]=V_{in}; \qquad [C_3]=[0 \quad 0 \quad 1 \quad 0 \quad 0 \quad 1 \quad 0]; \qquad [D_3]=[0]$$

The state equations derived above during ON period and OFF period of the switch are combined to obtain the following state space averaging model for the proposed hybrid single-switch DC-DC converter.

$$\begin{bmatrix} \dot{x} \end{bmatrix} = Ax + Bu; \qquad y = Cx + Du \tag{31}$$

Where, $[A]=A_1k+(A_2+A_3)(1-k)$; $[B]=B_1k+(B_2+B_3)(1-k)$;

$[C]=C_1k+(C_2+C_3)(1-k)$; $[D]=D_1k+(D_2+D_3)(1-k)$

$$[A]=\begin{bmatrix} 0 & 0 & 0 & -\frac{2(1-k)}{L_1} & 0 & 0 & 0 \\ 0 & 0 & 0 & \frac{k}{L_2} & \frac{2(1-k)}{L_2} & -\frac{(2-k)}{L_2} & -\frac{k}{L_2} \\ \frac{1-k}{(C_1+C_2)} & 0 & -\frac{1}{R_0}\left(\frac{1}{C_1}+\frac{1-k}{C_1+C_2}\right) & 0 & 0 & -\frac{1}{R_0}\left(\frac{1}{C_1}+\frac{1-k}{C_1+C_2}\right) & 0 \\ (1-k)\left(\frac{1}{C_2}+\frac{1}{C_1+C_2}\right) & -\frac{k}{C_2-C_3} & -\frac{(1-k)}{R_0(C_1+C_2)} & 0 & 0 & -\frac{(1-k)}{R_0(C_1+C_2)} & 0 \\ 0 & -\frac{k}{(C_2-C_3)}+\frac{2(1-k)}{(C_3+C_5)} & 0 & 0 & 0 & 0 & 0 \\ 0 & \frac{(2-k)}{C_4} & -\frac{(2-k)}{R_0C_4} & 0 & 0 & -\frac{(2-k)}{R_0C_4} & 0 \\ 0 & \frac{2(1-k)}{(C_3+C_5)}+\frac{k}{C_5} & 0 & 0 & 0 & 0 & 0 \end{bmatrix}$$

$$[B]=\begin{bmatrix} \frac{(2-k)}{L_1} & 0 & 0 & 0 & 0 & 0 & 0 \end{bmatrix}^T; \qquad [C]=[0 \quad 0 \quad (2-k) \quad 0 \quad 0 \quad (2-k) \quad 0]; \qquad [D]=[0]$$

## DESIGN OF CIRCUIT COMPONENTS

The power switch 'S' and the diodes $D_1$, $D_2$, $D_3$, and $D_4$ are assumed to be ideal semiconductor devices. The inductors ($L_1$ and $L_2$) and capacitors ($C_1$, $C_2$, $C_3$, $C_4$, and $C_5$) of the proposed hybrid converter

are designed for maximum values as the power switch 'S' has to support both the converter voltage and current.

***Design of inductors and capacitors***:

Assume that the input current ripple ($\Delta i_{L1}$) is 20% of input current ($i_{L1}$) and the output current ripple ($\Delta i_{L2}$) is 15% of load current ($I_0$). The duty ratio (k) of the power switch is 0.8. The switching frequency ($f_s$) is 10 kHz. The input voltage ($V_{in}$) is 24 V. The values of all inductors and capacitors used in the proposed converter are calculated as per the following expressions:

$$L_1 = \frac{V_{in}k}{f_s \Delta i_{L1}} = \frac{24 \times 0.8}{10 \times 10^3 \times \left(\frac{320}{24}\right) \times 0.2} = 0.72\,\text{mH}$$

$$L_2 = \frac{V_{in}k}{f_s \Delta i_{L2}} = \frac{0.8 \times 24}{10 \times 10^3 \times \left(\frac{320}{335}\right) \times 0.15} = 13.4\,\text{mH}$$

As the inductor values $L_1$ and $L_2$ are calculated as 0.72 mH and 13.4 mH respectively, it is assumed that an optimum value of 1 mH is selected for each of the inductors in the simulation study of the converter.

$$C_1 = \frac{V_0 k}{R_0 f_s \Delta V_{C1}} = \frac{335 \times 0.8}{320 \times 10 \times 10^3 \times 1.2} = 70\,\mu\text{F}$$

$$\Delta V_{C1} = \Delta V_{C2} = \Delta V_{C3} = \Delta V_{C5} = 1\% \text{ of } V_{C1} = \frac{1 \times V_{in}}{100(1-k)} = \frac{24}{100 \times 0.2} = 1.2\,\text{V}$$

The values of all the capacitors $C_1$, $C_2$, $C_3$, & $C_5$ are assumed as 80 µF each in the simulation study based on the above calculated value in order to have very low ripples in the capacitor voltages. Further, it is assumed that the capacitors $C_1$, $C_2$, $C_3$, & $C_5$ each have 1% voltage ripple. The value of capacitor $C_4$ is calculated as 0.8 µF as per the following formula in order to have low voltage ripple [22]. In the simulation study, its value is assumed as 1 µF.

$$C_4 = \frac{\Delta i_{L2}}{8 f_s \Delta V_{C4}} = \frac{\left(\frac{320}{335}\right) \times 0.15}{8 \times 10 \times 10^3 \times 2.16} = 0.8\,\mu\text{F}$$

$$\Delta V_{C4} = 1\% \text{ of } V_{C4} = \frac{1 \times (1+k) V_{in}}{100(1-k)} = \frac{1.8 \times 24}{100 \times 0.2} = 2.16\,\text{V}$$

## SIMULATION RESULTS AND DISCUSSION

The MATLAB / SIMULINK model of the proposed continuous input current hybrid single switch DC-DC converter structure as shown in Figure 5 is developed and simulated using variable-step type solver 'ode 45'. The switching frequency ($f_s$) of the converter is chosen as 10 kHz. The values of circuit parameters used for simulation are listed in Table I. The MOSFET switch S is triggered into conduction by a pulse width modulated gating pulse as shown in Figure 3. The range of variation of duty ratio 'D' of the MOSFET switch is taken as 0.5 < D < 0.9. Here, the simulation of the converter has been carried out with D = 0.8. A load of 320 W capacity with 320 Ω resistance is connected at the output of the converter. For simulation purpose, an input DC voltage ($V_{in}$) of magnitude 24 V is taken from a battery source as shown in Figure 6. The input current ($I_{in}$) waveform with steady state value of around 15 A is shown in Figure 7. The observation of output voltage ($V_0$) and output current ($I_0$) waveforms shown in Figure 8 and Figure 9 indicates that the approximate steady state values of $V_0$ = 335 V and $I_0$ = 1 A are reached after a small settling time of around 0.04 s. This output DC voltage ($V_0$) is 14 times the input DC voltage ($V_{in}$). The voltage and current waveforms for the two identical inductors $L_1$ and $L_2$ are shown in Figure 10, Figure 11, Figure 12, and Figure 13 respectively. The waveforms of voltage and current for the MOSFET switch are shown in Figure 14 and Figure 15 respectively which demonstrate that the switch S is subjected to low voltage and current stress. The voltage and current waveforms depicted in Figures 16 to Figure 23 for the four diodes $D_1$, $D_2$,

$D_3$, and $D_4$ indicate that the diodes too have low voltage-current stress. The voltage appearing across the capacitor $C_1$ ($V_{C1}$) is shown in Figure 24. According to the modes of operation of the converter, the capacitors $C_1$, $C_2$, $C_3$, and $C_5$ have the same steady state voltage magnitude ($V_{C1}$) of approximately 120 V appearing across each of them as shown in Figure 24. However, the capacitor $C_4$ has the steady state voltage magnitude ($V_{C4}$) of approximately 215 V appearing across it as illustrated in Figure 25. The waveforms of the currents through the capacitors $C_1$, $C_2$, $C_3$, $C_4$ and $C_5$ are shown in Figures 26 to Figure 30 respectively. The converter efficiency ($\eta_c$) is found to be 93% as calculated below:

$$\eta_c = \frac{P_0}{P_{in}} \times 100 = \frac{V_0 I_0}{V_{in} I_{in}} \times 100 = \frac{335 \times 1}{24 \times 15} \times 100 = 93\%$$

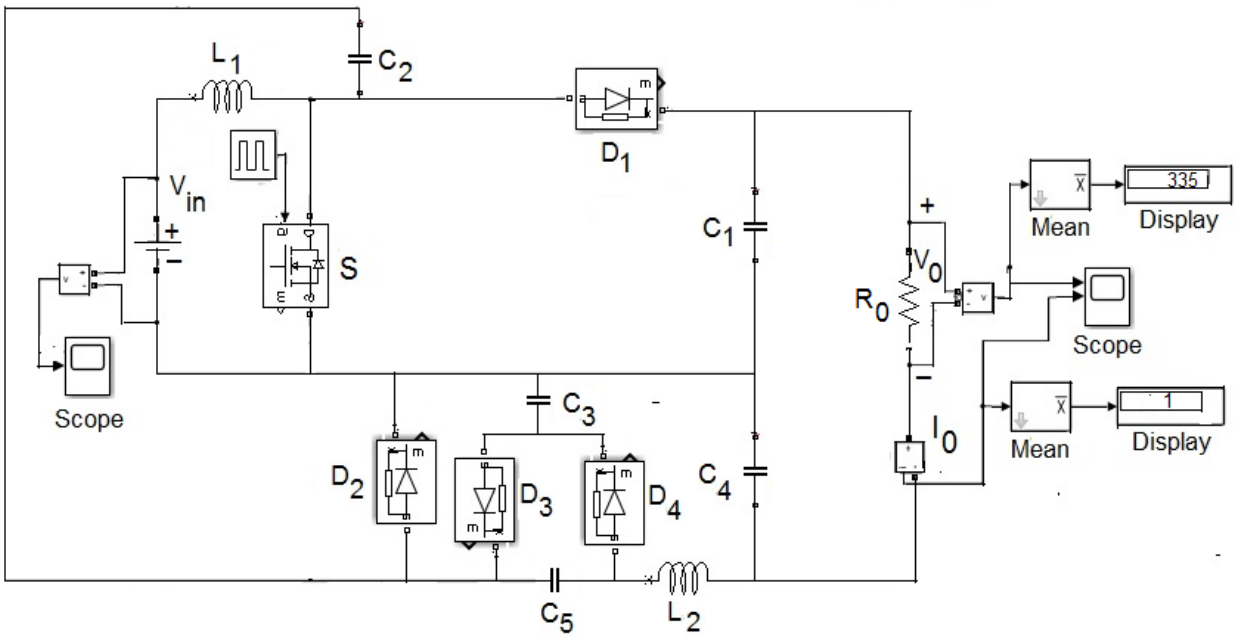


**Figure 5.** MATLAB / SIMULINK model of the proposed hybrid single switch DC-DC converter

**Table 1.** Parameters used for the simulation of the proposed hybrid DC-DC converter

| Parameters | Symbol | Value |
|---|---|---|
| Input voltage | $V_{in}$ | 24 V (DC) |
| Output voltage | $V_0$ | 335 V (DC) |
| Inductors | $L_1$, $L_2$ | 1 mH each |
| Capacitors | $C_1$, $C_2$, $C_3$, $C_5$ | 80 µF each |
| Capacitor | $C_4$ | 1 µF |
| Switching frequency | $f_s$ | 10 kHz |
| Load resistance | $R_0$ | 320 Ω |
| Load power | $P_0$ | 320 W |
| Average output current | $I_0$ | 1 A |
| Duty ratio of the switch | D | 0.8 |

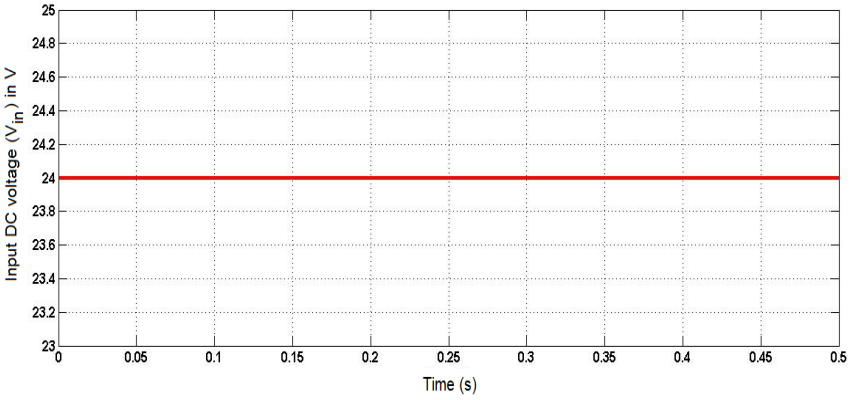


**Figure 6.** Input DC voltage ($V_{in}$)

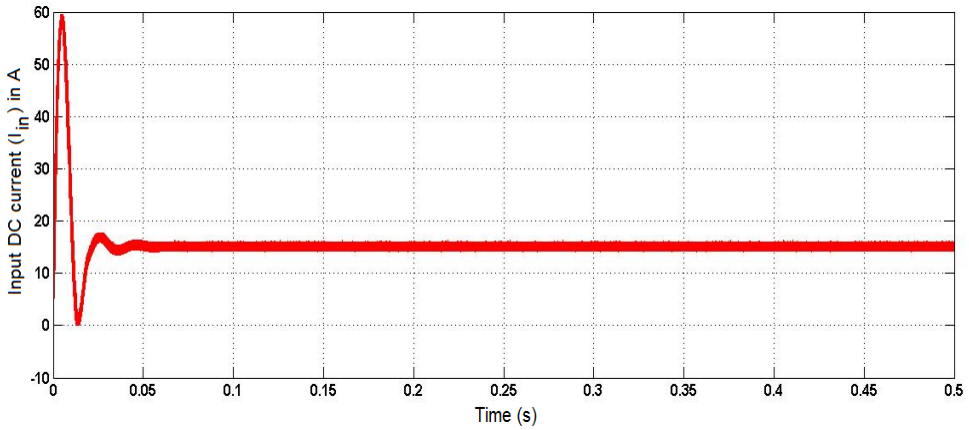


**Figure 7.** Input DC current ($I_{in}$)

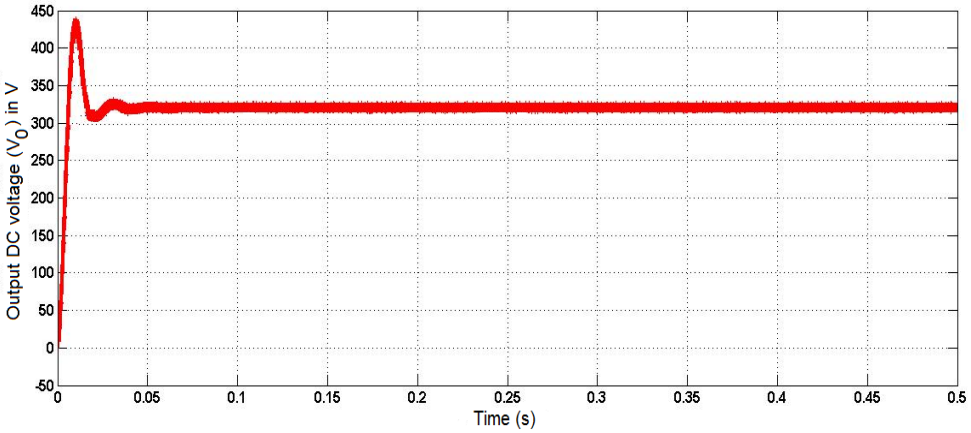


**Figure 8.** Output DC voltage ($V_0$)

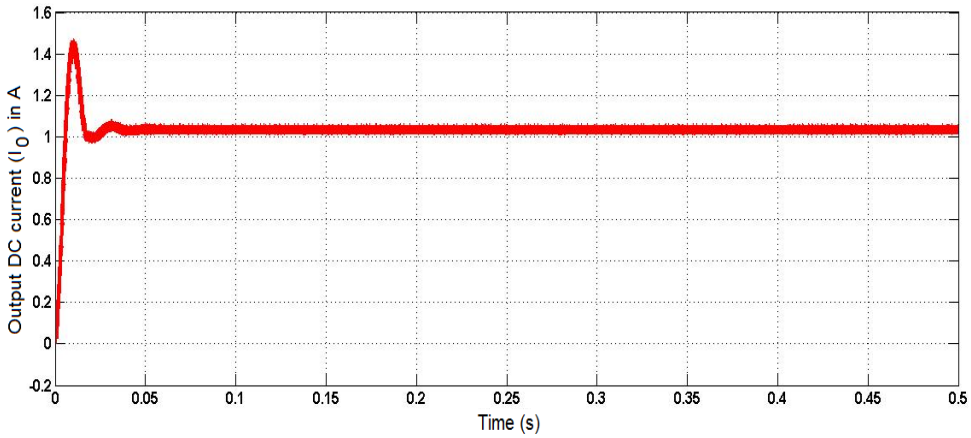


**Figure 9.** Output DC current ($I_0$)

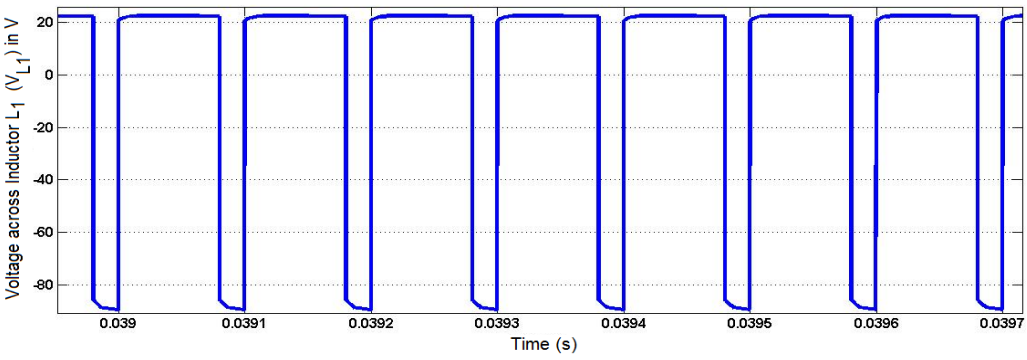


**Figure 10.** Voltage across inductor $L_1$ ($V_{L1}$)

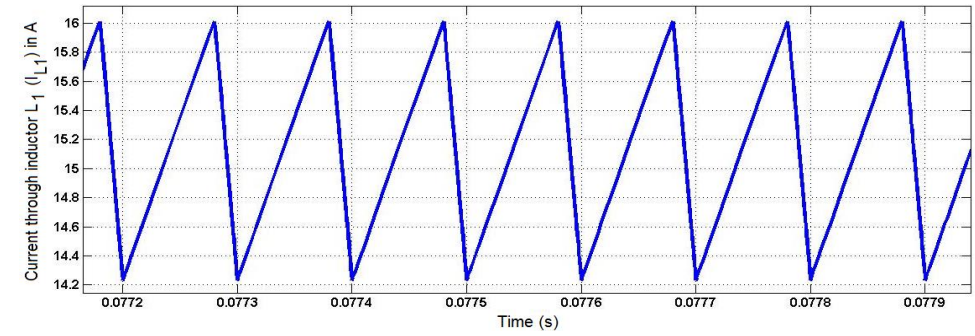


**Figure 11.** Current through inductor $L_1$ ($I_{L1}$)

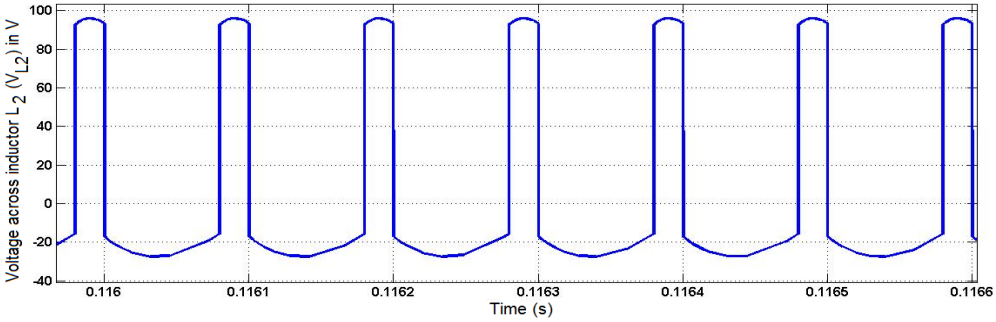


**Figure 12.** Voltage across inductor $L_2$ ($V_{L2}$)

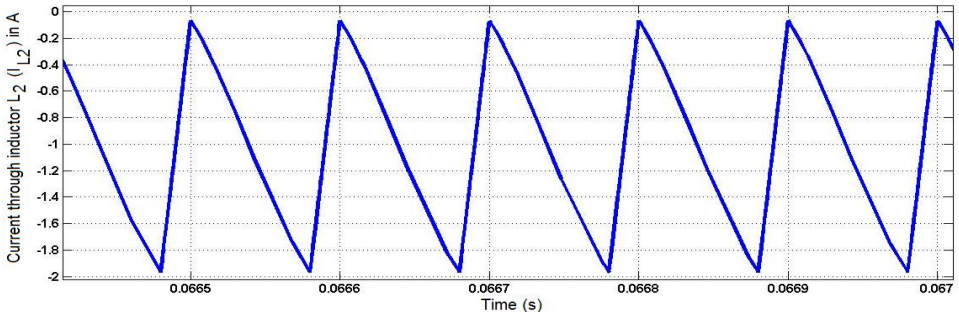


**Figure 13.** Current through inductor $L_2$ ($I_{L2}$)

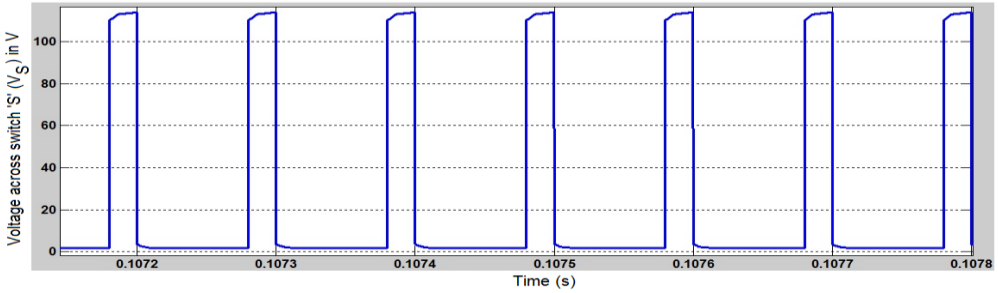


**Figure 14**. Voltage across switch 'S' ($V_S$)

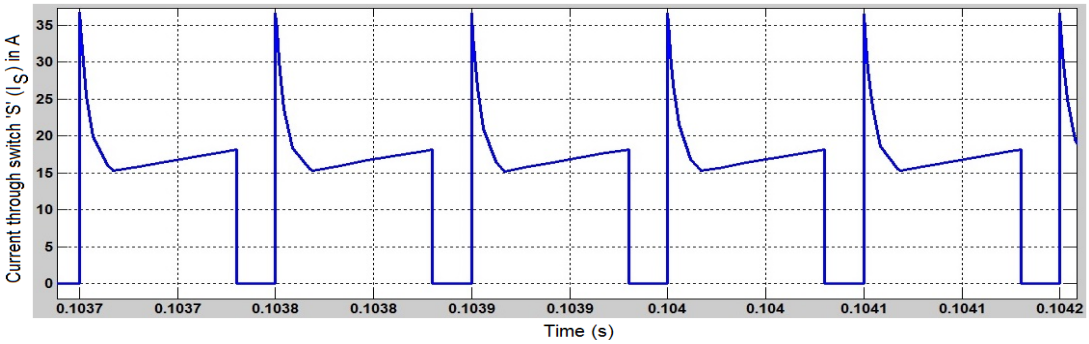


**Figure 15.** Current through switch 'S' ($I_S$)

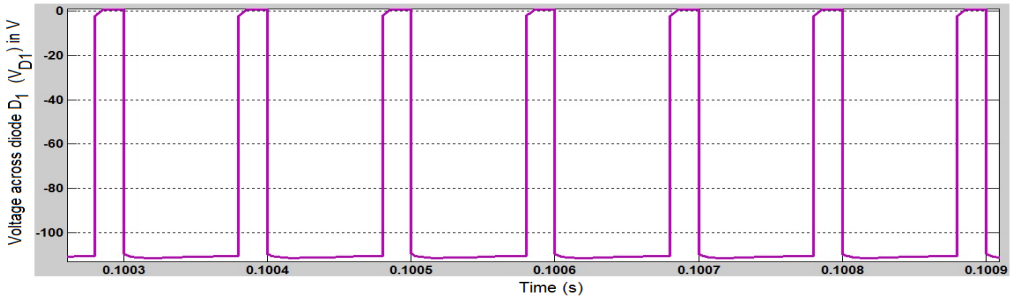


**Figure 16.** Voltage across diode $D_1$ ($V_{D1}$)

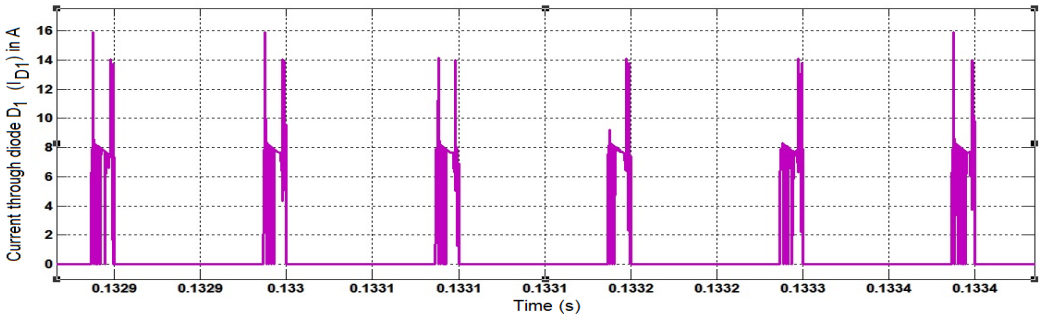


**Figure 17.** Current through diode $D_1$ ($I_{D1}$)

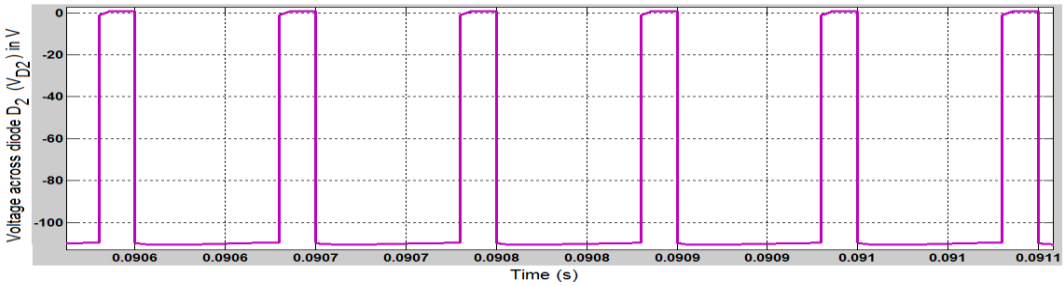


**Figure 18.** Voltage across diode $D_2$ ($V_{D2}$)

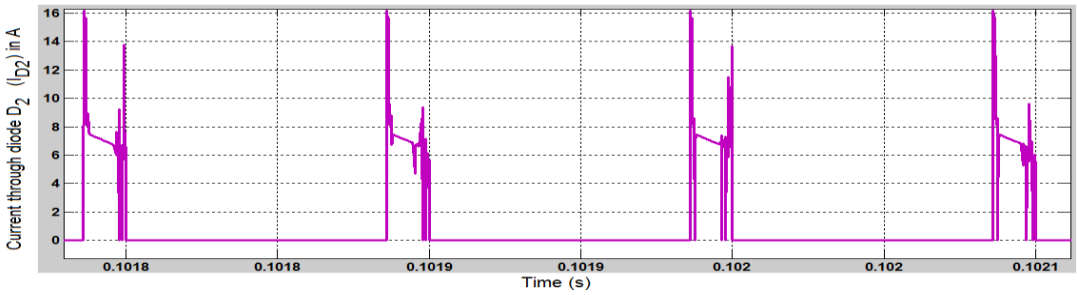


**Figure 19**. Current through diode $D_2$ ($I_{D2}$)

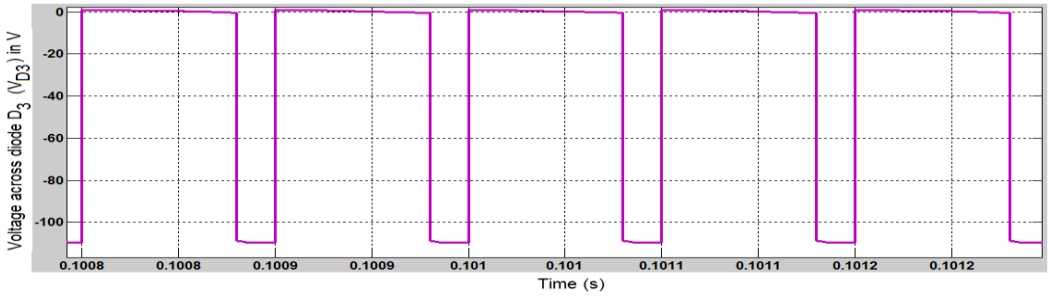


**Figure 20**. Voltage across diode $D_3$ ($V_{D3}$)

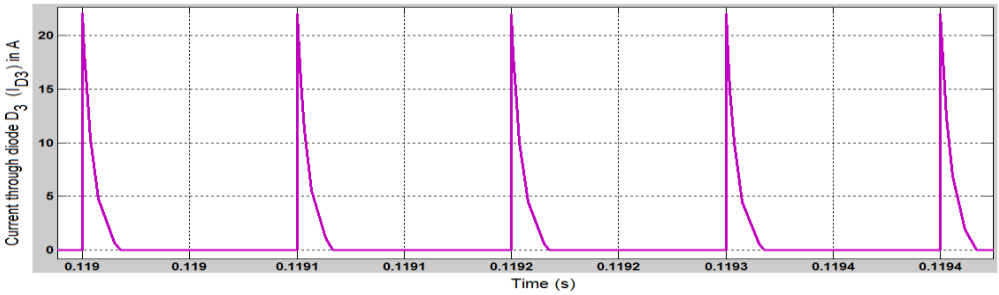


**Figure 21.** Current through diode $D_3$ ($I_{D3}$)

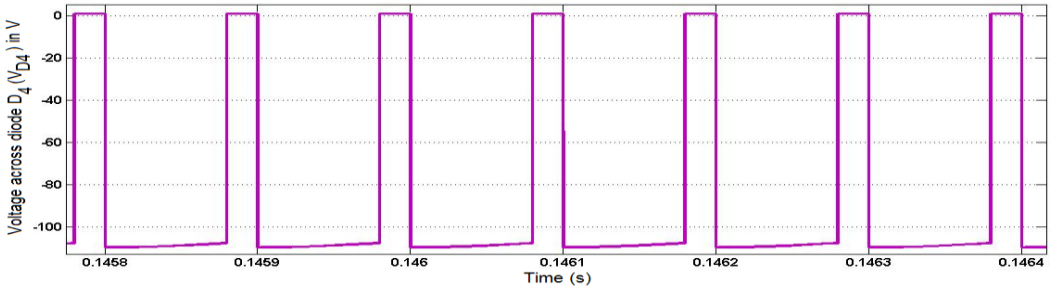


**Figure 22.** Voltage across diode $D_4$ ($V_{D4}$)

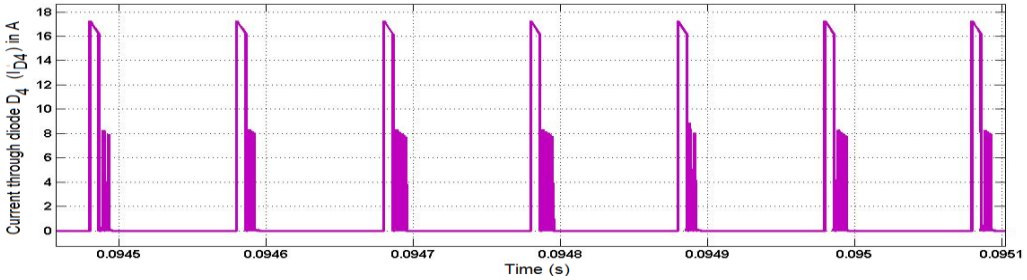


**Figure 23.** Current through diode $D_4$ ($I_{D4}$)

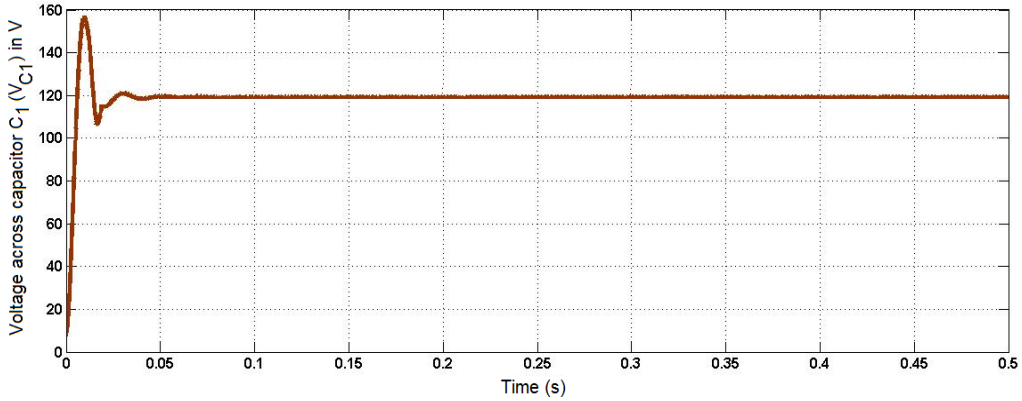


**Figure 24.** Voltage across capacitor $C_1$ ($V_{C1} = V_{C2} = V_{C3} = -V_{C5}$)

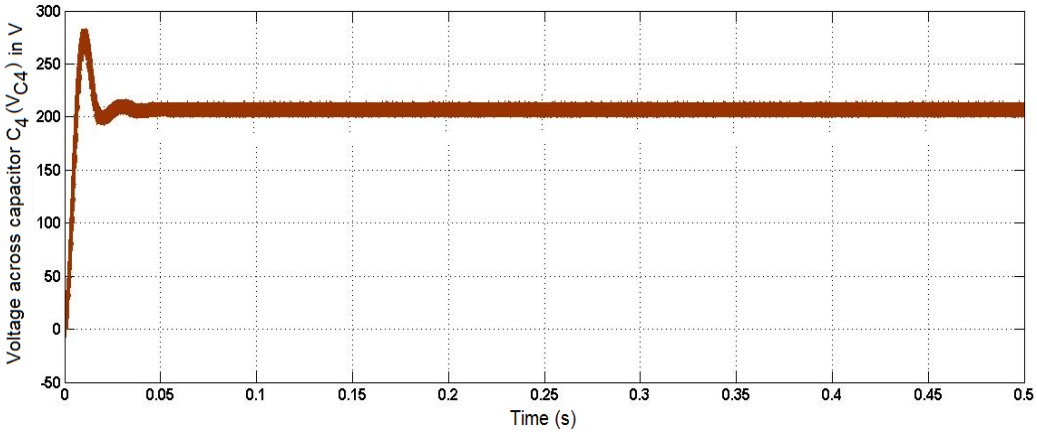


**Figure 25.** Voltage across capacitor $C_4$ ($V_{C4}$)

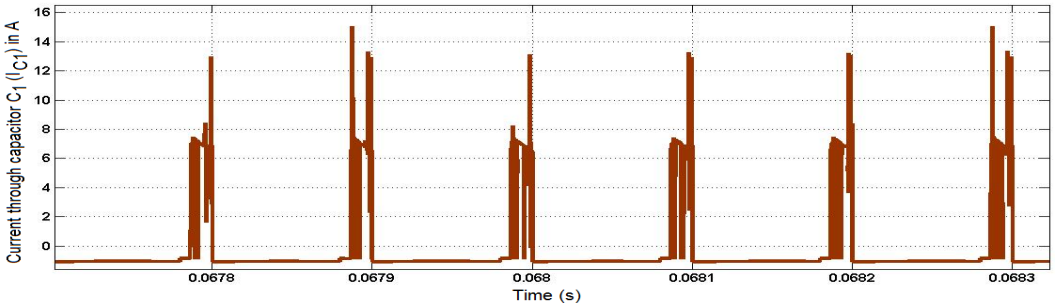


**Figure 26.** Current through capacitor $C_1$ ($I_{C1}$)

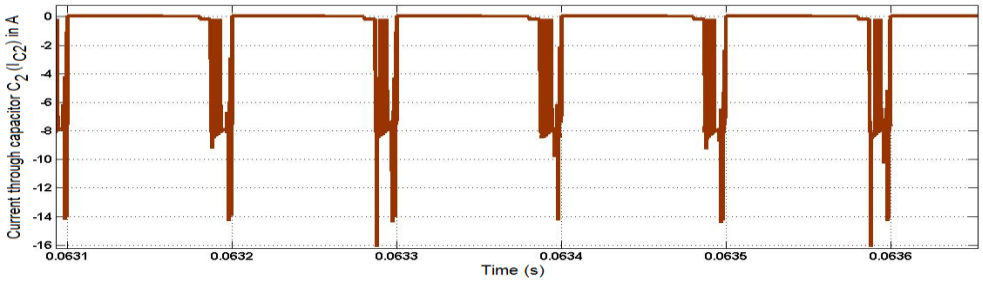


**Figure 27.** Current through capacitor $C_2$ ($I_{C2}$)

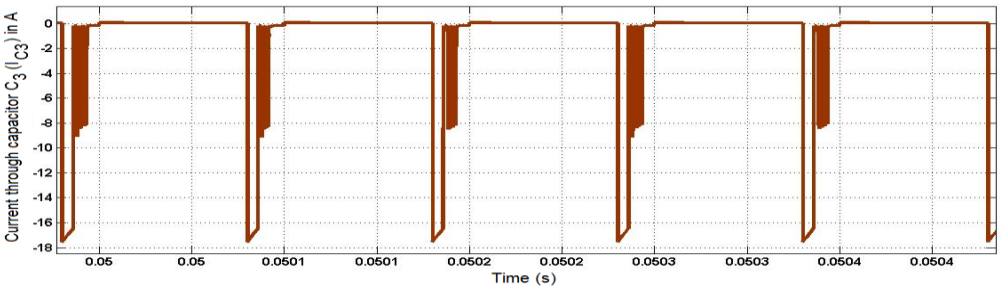


**Figure 28.** Current through capacitor $C_3$ ($I_{C3}$)

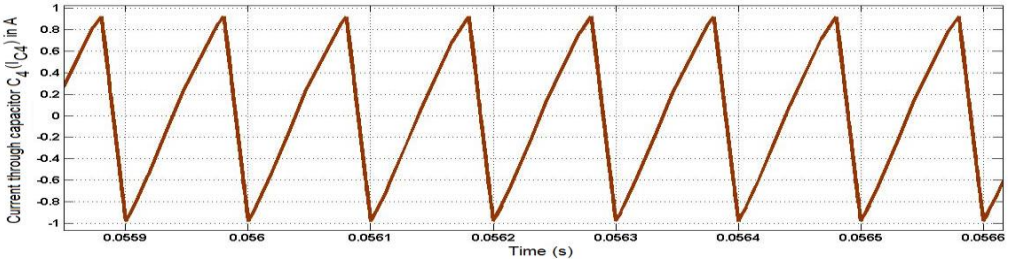


**Figure 29.** Current through capacitor $C_4$ ($I_{C4}$)

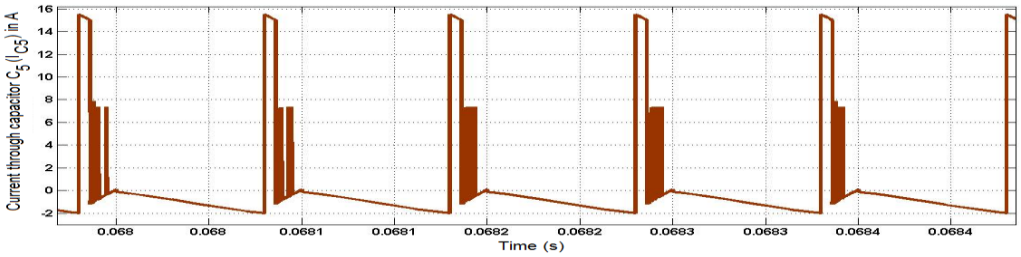


**Figure 30.** Current through capacitor $C_5$ ($I_{C5}$)

## CONCLUSION

In this paper, the steady state behavior of a non-isolated hybrid single-switch high step-up positive output DC-DC converter operating in continuous inductor current mode has been explored. The proposed hybrid topology is the integrated structures of conventional boost converter and modified CUK converter. The performance of the converter is validated through MATLAB / SIMULINK study. The waveforms of voltage and current for the power switch, diodes, inductors, capacitors, and load are presented and analyzed for the converter with power switch duty ratio D = 0.8. The simulation results prove the effectiveness of the proposed hybrid single-switch topology in improving the static voltage gain by (2+D) times that of the traditional boost converter. The power conversion efficiency of the converter is calculated as 93%. The voltage-current stress on the single power switch and the diodes is found to be low. Moreover, only few oscillations are observed on the output voltage and current waveforms before they settle down to steady state. The filter capacitors $C_1$ and $C_4$ are so selected that the percentage of ripples present in the output voltage and output current is very low. The state space averaging model of the proposed hybrid converter is also detailed. The proposed hybrid single-switch DC-DC converter configuration is more suitable for renewable energy applications requiring improved voltage gain and high power conversion efficiency.

**Funding:** This research received no external funding.
**Acknowledgments:** The author acknowledges the technical support provided by the Department of Electrical and Electronics Engineering, Government College of Engineering, Salem, in carrying out the simulation work on the proposed converter.
**Conflicts of Interest:** The author declares no conflict of interest.

## REFERENCES

1. Acar C, Dincer I. Environmental impact assessment of renewable and conventional fuels for different end use purposes. Int J Global Warming. 2017 Jan; 13(3/4):260-77.
2. Perera F. Pollution from fossil-fuel combustion is the leading environmental threat to global pediatric health and equity: Solutions exist. Int J Environ Res Public Health. 2018 Jan; 15(1):1-17.
3. Colmenar-Santos A, Monteagudo-Mencucci M, Rosales-Asensio E, de Simon-Martin M, Perez-Molina C. Optimized design method for storage systems in photovoltaic plants with delivery limitation. Solar Energy, 2019 Mar; 180:468-88.
4. Ma T, Javed MS. Integrated sizing of hybrid PV-wind-battery system for remote island considering the saturation of each renewable energy resource. Energy Convers Manag. 2019 Feb; 182:178-90.
5. Kolli A, Gaillard A, De Bernardinis A, Bethoux O, Hissel D, Khatir Z. A review on DC/DC converter architectures for power fuel cell applications. Energy Convers Manag. 2015 Nov; 105:716-30.
6. Sivakumar S, Sathik MJ, Manoj PS, Sundararajan G. An assessment on performance of DC-DC converters for renewable energy applications. Renew Sustain Energy Rev. 2016 May; 58:1475-85.
7. Gopi A, Saravanakumar R. High step-up isolated efficient single switch DC-DC converter for renewable energy source. Ain Shams Eng J. 2014 Dec; 5(4):1115-27.
8. Liang TJ, Lee JH, Chen SM, Chen JF, Yang LS. Novel isolated high step-up DC-DC converter with voltage lift. IEEE Trans Ind Electron. 2013 Apr; 60(4):1483-91.
9. Alsaleem A, Alsakran F, Simoes MG. An isolated high voltage boost current-fed DC-DC converter based on 1:1 transformer multiplier cells and ZVS operation. Electronics, 2020 Jan; 9(1):1-15.
10. Nymand M, Andersen MAE. High-efficiency isolated boost DC-DC converter for high-power low-voltage fuel-cell applications. IEEE Trans Ind Electron. 2010 Feb; 57(2):505-14.
11. Mumtaz F, Yahaya NZ, Meraj ST, Singh B, Ramani Kannan, Ibrahim O. Review on non-isolated DC-DC converters and their control techniques for renewable energy applications. Ain Shams Eng J. 2021 Dec; 12(4):3747-63.
12. Tofoli FL, de Castro Pereira D, de Paula WJ, de Sousa Oliveira Junior D. Survey on non-isolated high-voltage step-up dc-dc topologies based on the boost converter. IET Power Electronics, 2015 Oct; 8(10):2044-57.

13. Maroti PK, Esmaeili S, Iqbal A, Meraj M. High step-up single switch quadratic modified SEPIC converter for DC microgrid applications. IET Power Electronics, 2020 Dec; 13(16):3717-26.
14. Murali D. Steady state behavior of a single-switch non-isolated DC-DC SEPIC converter topology with improved static voltage gain. J Eur Syst Autom, 2021 June; 54(3):445-52.
15. Maroti PK, Sanjeevikumar P, Wheeler P, Blaabjerg F, Rivera M. Modified high voltage conversion inverting Cuk DC-DC converter for renewable energy application. Proceedings of the 3rd IEEE Annual Southern Hemisphere Conference on Power Electronics (IEEE-SPEC'17), Puert Varas (Chile), 2017; 173-77. doi.org/10.1109/SPEC.2017.8333675.
16. Zhu B, Liu G, Zhang Y, Huang Y, Hu S. Single-switch high step-up Zeta converter based on Coat circuit. IEEE Access, 2020 Dec; 99:1-11.
17. Dahono PA. Derivation of high voltage-gain step-up DC-DC power converters. Int J Electr Eng Inform. 2019 June; 11(2):236-51.
18. De Souza JP, de Oliveira P, Gules R, Romaneli EFR, Badin AA. A high static gain CUK DC-DC converter. Proceedings of the 13th IEEE Brazilian Power Electronics Conference and 1st Southern Power Electronics Conference (COBEP/SPEC), 2015; 1-6. doi.org/10.1109/COBEP.2015.7420064.
19. Murali D, Annapurani S. Improvement of static voltage gain of a non-isolated positive output single-switch DC-DC converter structure using a diode-capacitor cell. Math Model Eng Probl. 2021 Aug; 8(4):583-90.
20. Chandran IR, Ramasamy S, Ahsan M, Haider J, Rodrigues EMG. Implementation of non-isolated Zeta-KY triple port converter for renewable energy applications. Electronics, 2021 July; 10(14):1-28.
21. Jayanthi K, Senthil Kumar N, Gnanavadivel J. Design and implementation of modified SEPIC high-gain DC-DC converter for DC microgrid applications. Int Trans Electr Energy Syst. 2021 Aug; 31(8):2100-18.
22. Karthikeyan M, Elavarasu R, Ramesh P, Bharatiraja C, Sanjeevikumar P, Mihet-Popa L, Mitolo M. A hybridization of Cuk and Boost converter using single switch with higher voltage gain capability. Energies, 2020 May; 13(2312):1-24.
23. Manish Kumar, Ashirvad M, Narendra Babu Y. An integrated Boost-Sepic-Cuk DC-DC converter with high voltage ratio and reduced input current ripple. Energy Procedia, 2017 June; 117:984-90.
24. Gupta N, Almakhles D, Bhaskar Ranjana MS, Sanjeevikumar P, Holm-Nielsen JB, Mitolo M. Novel hybrid high gain converter: Combination of Cuk and buck-boost structures with switched inductor for DC microgrid. 2nd IEEE Global Power, Energy and Communication Conference (GPECOM), 2020; 1-7. doi.org/10.1109/GPECOM49333.2020.9247912.